International Journal of Heat and Mass Transfer 202 (2023) 123769

Contents lists available at ScienceDirect

International Journal of Heat and Mass Transfer

journal homepage: www.elsevier.com/locate/hmt

# Shape optimization of pin fin array in a cooling channel using genetic algorithm and machine learning

Nam Phuong Nguyen[a], Elham Maghsoudi[b], Scott N. Roberts[b], Beomjin Kwon[a,*]

[a] School for Engineering of Matter, Transport and Energy, Arizona State University, Tempe, AZ 85287, USA
[b] NASA Jet Propulsion Laboratory, California Institute of Technology, Pasadena, California 91109, USA

ARTICLE INFO

*Article history:*
Received 8 August 2022
Revised 4 December 2022
Accepted 8 December 2022
Available online 18 December 2022

*Keywords:*
Pin fin
Shape optimization
Genetic algorithm
Machine learning model

ABSTRACT

This article reports the optimization of pin fin shape using a genetic algorithm (GA) coupled either to a machine learning (ML) model or a computational fluid dynamics (CFD) model. The ML model evaluates the temperature and pressure induced by the fins within a second and allows us to replace the time-consuming CFD simulations during the design stage. The optimization is conducted for a cooling channel with a uniform heat flux boundary condition (5 W/cm$^2$) in the Reynolds numbers range of 3000 – 12000. The optimization identifies a funnel-shaped fin that enhances the heat transfer coefficient by 20% without an apparent increase of pressure drop as compared to the standard cylindrical pin fins. The funnel-shaped fin outperforms other conventional fins of elliptical, cubic, and drop shapes that induce a similar level of pressure drops. This work demonstrates the potential of ML-based optimization in searching unexplored shapes of heat transfer systems with superior performance.



## 1. Introduction

The advances in integrated, miniaturized, and power electronic devices are imposing challenges for cooling and thermal management technologies since there are growing demands to reject substantial heat fluxes (e.g., > 100 W/cm$^2$) and operate the devices under extreme environmental conditions (e.g., space) [1,2]. One of the common strategies to improve the cooling rates of heat transfer systems is to increase the heat transfer coefficient and surface area by integrating pin fin arrays. Extensive research has been conducted to understand the relationship between the pin fin geometries and their heat transfer performance and pressure drop [3–7]. When employing the pin fins with noncircular cross-sections such as square, cubic, and oblong-shaped ones, in general, fins induce greater vortices and improve the heat transfer performance (e.g., < 20%) as compared to the standard circular pin fins despite the apparent increases of the pressure drop penalty (e.g., < 200%) [3–5]. In contrast, there are other types of fins like drop-shaped and perforated pin fins that are known to considerably reduce the pressure drop penalty (e.g., < 20%) without apparent enhancement of the heat transfer coefficients than the circular pin fins [6,7]. Despite the considerable research on the pin fin shapes that are both thermally and hydrodynamically efficient, still, conventional geometries are popular in practice because these forms are not expensive to make and are easy to derive from our intuition.

To search unexplored design space for pin fins, there have been efforts to leverage the recent advances in optimization and manufacturing. A typical objective of cooling system design is to maximize the heat transfer performance while minimizing the pressure drop penalty. Due to the highly complex nature of the fluid-heat-structure interactions, the heat transfer systems are commonly optimized through gradient-free methods instead of the fast gradient-based methods which require computing the gradients of the objective functions. A popular gradient-free method is to combine the genetic algorithm (GA) and computational fluid dynamics (CFD) [8–11]. The GA randomly generates designs through an artificial biological evolution process involving mutation, recombination, and reproduction steps then compares the designs and finds an optimal solution. The CFD simulation is used to predict the heat transfer performances and the pressure drops of the generated designs that determine the objective function (denoted as a fitness function in GA) of the optimization problem. In a recent demonstration [10], a three-dimensional (3D) printed heat sink integrated with rectangular fins was designed by a GA-based approach. By optimizing the shape of the coolant flow passage, the heat transfer coefficient was enhanced by nearly 15% while the heat sink weight was reduced by up to 30% compared to the conventional design [10]. Similarly, the GA was used to derive non-standard, spear-shaped internal fins in a tube-in-tube heat exchanger that improved the heat transfer coefficient up to 200% while limiting

* Corresponding author.
*E-mail address:* kwon@asu.edu (B. Kwon).

https://doi.org/10.1016/j.ijheatmasstransfer.2022.123769
0017-9310/

**Nomenclature**

| | |
|---|---|
| $c_p$ | specific heat, J/Kg K |
| $D_h$ | channel hydraulic diameter, m |
| $f$ | Darcy friction factor, dimensionless |
| $f_0$ | Darcy friction factor of the cylindrical pin fin, dimensionless |
| $F$ | fitness function, dimensionless |
| $h$ | convective heat transfer coefficient, W/m$^2$K |
| $h_0$ | convective heat transfer coefficient of the cylindrical pin fin, W/m$^2$K |
| $H$ | height of channel, m |
| $i$ | iterative number, dimensionless |
| $i_{max}$ | maximum iterative number, dimensionless |
| $L$ | length of channel, m |
| $\Delta P$ | pressure drop between the inlet and outlet of the channel, Pa |
| $q$" | heat flux, W/cm$^2$ |
| $R^2$ | determination of coefficient, dimensionless |
| $Re$ | Reynolds number, dimensionless |
| $S_l$ | longitudinal spacing of pin fins, m |
| $S_t$ | transverse spacing of pin fins, m |
| $T$ | heated surface temperature, K |
| $T_i$ | inlet temperature of fluid, K |
| $T_m$ | bulk mean temperature of fluid, K |
| $\Delta T$ | temperature difference between heated surface and the flow inlet, K |
| $u$ | average flow velocity, m/s |
| $W$ | width of channel, m |

*Greek symbol*

| | |
|---|---|
| $\alpha$ | thermal diffusivity, m$^2$/s |
| $\lambda$ | weight parameter, dimensionless |
| $\eta$ | efficiency index, dimensionless |
| $\rho$ | density, kg/m$^3$ |
| $\mu$ | dynamic viscosity, kg/ms |

the pressure increase to merely less than 5% [12]. Despite the promising potential, the design method using GA and CFD demands extensive computation time, which has been limiting the widespread use of this technique [13]. Through the iterative process, the GA generates a large number of designs, and the CFD simulation evaluates the designs over a substantial time (e.g., a day or longer).

To reduce the computation time of the GA approach, an alternative method is desired to rapidly evaluate the generated designs. Recently, machine learning (ML) techniques have been explored as rapid prediction methods for complex thermofluidic phenomena [14–16]. For example, the random forests (RF) algorithm was used to automatically classify the flow images taken from a 3D printed wavy tube according to the flow regime with an accuracy of up to 95% [17]. Another demonstration used convolutional neural networks (CNNs) to predict the heat flux of pool boiling from the snapshots of boiling water [18]. The model successfully labeled the boiling mechanism such as nucleation, coalescence, and departure to the snapshots of boiling water with a mean error of 6% [18]. In a previous work [19], the RF was trained to predict the local heat transfer coefficient in a cooling channel integrated with rib roughness with an accuracy greater than 0.996 [19]. The aforementioned examples demonstrate the utility of ML techniques for thermofluidic problems since the trained ML models can rapidly infer the solutions from the provided high-dimensional data (e.g., data having many input variables) and unstructured data (e.g., data that is not organized in a predefined manner such as images). Therefore, there is a great opportunity in ML techniques as the rapid evaluation method for thermofluidic devices, which has not yet been widely explored.

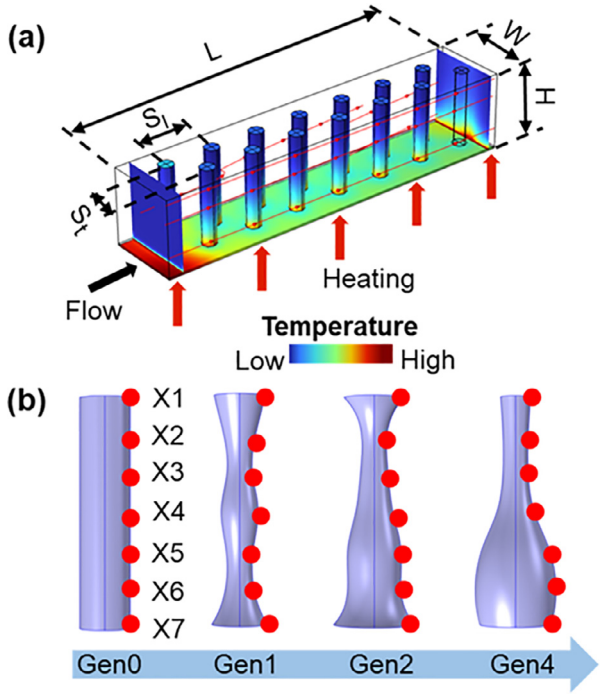


**Fig. 1.** (a) Schematic of a channel under external heating showing the geometric parameters. (b) Evolution of the pin fin geometry defined by 7 control points (X1 – X7). Gen represents the generation or iteration of the iterative design process.

This work aims to optimize the shape of pin fins integrated into a cooling channel using the GA. The generated designs are evaluated by two different methods: (1) three-dimensional (3D) CFD simulation and (2) RF surrogate model. We compare the designs generated by the two design evaluators and discuss the opportunities with ML-assisted optimization.

## 2. Pin Fin Design Overview

Fig. 1(a) shows 7 rows of staggered cylindrical pin fins in a channel with a square cross-section. The channel is 20 mm in width ($W$) and height ($H$), and 100 mm in length ($L$). The channel bottom surface is subject to uniform heat flux, $q$" = 5 W/cm$^2$, while the side and top surfaces are insulated. A fully developed water flow at 300 K enters the channel inlet. The water velocity ($u$) is in the range of 0.13 - 0.5 m/s which leads to the Reynolds number ($Re$) of 3040 - 11790. For the pin fin array, transverse spacing ($S_t$) is 7 mm and longitudinal spacing ($S_l$) is 13 mm. Fig. 1a also illustrates an exemplary temperature map predicted by a CFD simulation, showing how the pin fins contribute to cooling down the heated surface by extending the surface area and creating wakes [20,21].

For optimizing the pin fin geometry, we first define 7 control points (X1 to X7) along the vertical profile as shown in Fig. 1(b). The control points are equally spaced in the vertical direction, but allowed to move in the horizontal direction within a radial position of 2 - 7 mm. The control points are connected by a smooth interpolated curve to form a vertical profile, which is then revolved to generate a 3D model of a pin fin. This interpolating method has been reported to preserve the shape of data and well avoid an overshoot relatively.

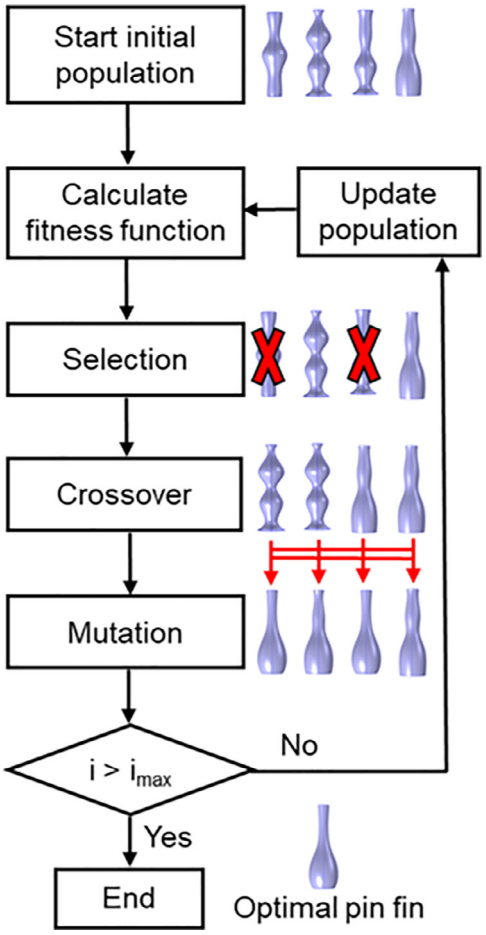


**Fig. 2.** Flowchart of the genetic algorithm-based optimization.

## 3. Optimization with GA and Finite Element Model

The GA is developed to derive an optimal pin fin shape that minimizes a fitness function $F = \lambda T + \Delta P$, where $\lambda$ is the weight on the average temperature of the heated surface ($T$) in Kelvin and $\Delta P$ is the pressure drop across the channel in Pascal. The minimization of fitness function identifies the optimal fin volume that balances the heat transfer performance and the pressure drop penalty. Fig. 2 shows a flowchart of the GA that starts by randomly generating a population of pin fin profiles. The generated pin fin profiles are transferred to a 3D finite element model (FEM) that calculates the velocity and temperature fields of the flow as well as $T$, $\Delta P$, and $F$ only at $Re = 3040$. We implemented the GA using MATLAB R2018a and the 3D FEM using COMSOL Multiphysics 6.0. The FEM solved the continuity, momentum, and energy equations for steady-state incompressible flow under Boussinesq approximation that are shown below.

$$\nabla \cdot \vec{u} = 0 \tag{1}$$

$$\rho(\vec{u} \cdot \nabla \vec{u}) = -\nabla P + \nabla \cdot (\mu \nabla \vec{u}) \tag{2}$$

$$\rho c_p \left(\vec{V} \cdot \nabla T\right) = \alpha \nabla^2 T \tag{3}$$

The generation process of the pin fin profiles mimics the biological evolutionary phases including selection, crossover, and mutation [22]. In this process, each pin fin design is encoded in a chromosome as a bit string. In the selection step, a portion of pin fin profiles with a small $F$ is likely to be selected. In the crossover step, the selected parent's chromosomes exchange their characteristics for creating their children's chromosomes. Then, the parts of the children's chromosomes are randomly modified to diversify the population, which provides a mechanism for escaping from a local minimum. As a result, a new generation of pin fin designs that inherit superior chromosomes from the previous generation is produced. The evolution process is repeated until the iteration number ($i$) reaches the maximum limit ($i_{max}$).

## 4. Effect of population size and weight on optimization

The population size and weight ($\lambda$) are important parameters of the GA. The population size determines how many design candidates are compared in each generation. $\lambda$ represents how much the designer considers $T$ more important than $\Delta P$, which is a subjective criterion. To understand the effect of these parameters, two population sizes (i.e., 15 and 25) and three values of $\lambda$ (i.e., 0.2, 4, and 7) are tested.

Fig. 3 shows the best $F$ over 10 generations of evolution. With any $\lambda$, $F$ obtained with a population size of 25 is 1% - 7% smaller

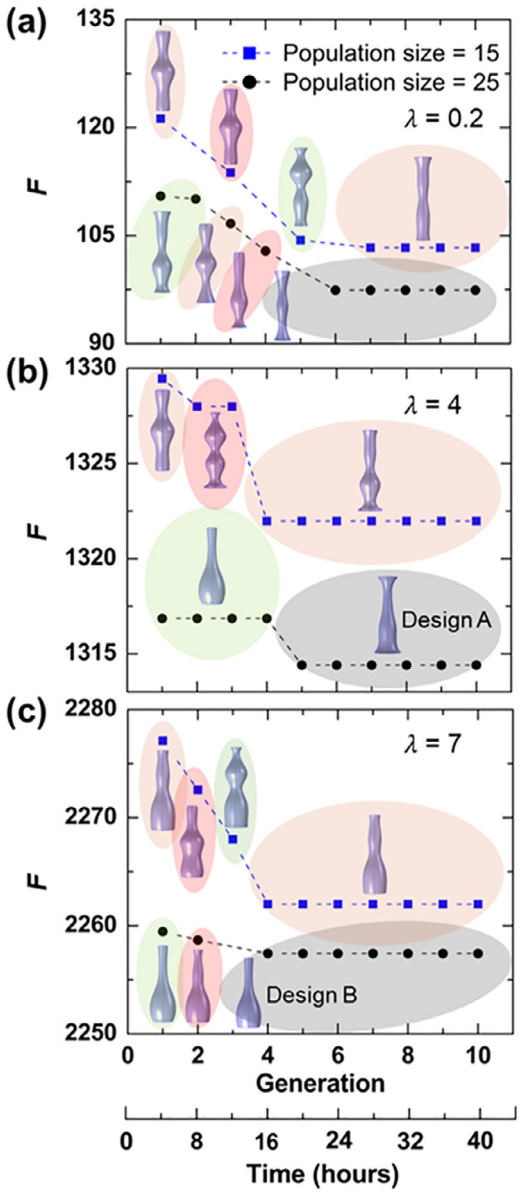


**Fig. 3.** Fitness function, $F$, over generations and computation time when $\lambda$ was selected as (a) 0.2, (b) 4, and (c) 7. For the design exploration, FEM served the design evaluator, and two different population sizes were tested.

than $F$ obtained with a population size of 15, meaning that a sufficient initial population size is needed for finding better solutions. However, the increase in the population would significantly extend the computation time, since FEM needs to evaluate more design candidates. For instance, the optimization took around 24 hours with a population of 15 and took around 40 hours with a population of 25 in our computer setting to complete 10 generations. Fig. 3 shows that the choice of a small $\lambda$ (i.e., $\lambda = 0.2$) produces the designs with narrow pin diameters while the choice of a large $\lambda$ (i.e., $\lambda = 7$) creates the designs with wide bottom areas. The pin fins with narrow cross-sectional areas induce small $\Delta P$, and they do not transfer heat as much as the pin fins with wide cross-sectional areas. The pin fins with wide bottom areas effectively extract heat from the heated surface to the surrounding coolant while preventing an excessive $\Delta P$ due to the slim upper areas. We also tested other values of $\lambda$ such as 0, 1, 3, 5, 6,8, 10, and 100. However, the solutions from $\lambda = 1$ and 3 were not significantly different than the solution from $\lambda = 0.2$. The optimal designs from $\lambda = 5$ and 6 were similar to the solution from $\lambda = 4$. The solution from $\lambda = 10$ was similar to the solution from $\lambda = 7$. The optimization with $\lambda$ of 0 and 100 correspond to two limiting cases. The solution from $\lambda = 0$ produces the pin fin with a minimum diameter (i.e., 2 mm) everywhere, since the small fin cross-sectional area minimizes the flow resistance. By contrast, the solution from $\lambda = 100$ produces the pin fin with a maximum diameter (i.e., 7 mm), since the large fin cross-sectional area maximizes the heat conduction from the heated surface to fin tip. These two limiting cases present intuitive designs per our understanding on heat transfer and fluid physics.

Through the test of population size and $\lambda$, we identified two interesting designs at $\lambda = 4$ (denoted as design A) and $\lambda = 7$ (denoted as design B) when the population size was 25. Design A has an average diameter of 4.17 mm with a standard deviation of 1.57 mm and design B has an average diameter of 4.17 mm with a standard deviation of 1.92 mm. Design B has a similar shape to the optimal pin fins reported by previous studies [23,24]. The previous works optimized the shape of pin fin under natural, laminar, and turbulent convections without fixing the pumping power. Particularly, in [24] the objective was to minimize thermal resistance and pressure drop. These works validate the outcomes of our optimization. For the two designs, A and B, FEM was used to compute $\Delta P$ and $T$ in the full range of $Re$ (i.e., $Re$ = 3040 - 11790) to understand how the optimal pin fins improved the cooling channel characteristics. To minimize the sensitivity of the simulation results to the grid size, a mesh independence test was performed by employing five different numbers of mesh elements, ranging from $50 \times 10^3$ to $3.1 \times 10^6$. The test showed that the calculated $\Delta P$ and $T$ differed less than 1% when the grid size was greater than $90 \times 10^4$. Thus, all the subsequent FEM simulations were obtained with the mesh number of $90 \times 10^4$.

Fig. 4 compares $\Delta P$ and the increase in surface temperature ($\Delta T$) of the cooling channels integrated with the optimally designed pin fins along with two reference cooling channels. $\Delta T$ is calculated by $\Delta T = T - T_i$, where $T_i$ is the inlet water temperature. The reference channels are the channel with standard cylindrical pin fins with a diameter of 4 mm (denoted as the cylindrical fin channel) and the channel without any pins (denoted as a plain channel). As compared to the cylindrical fin channel, design A reduces $\Delta P$ nearly by 12% while design B show a great similarity of $\Delta P$. In the plain channel, $\Delta P$ is less than 2 Pa, since there is no fin-induced flow swirling. Fig. 4b shows that $\Delta T$ is 50°C in the plain channel while $\Delta T$ reduces to 15.9°C in design A, to 17.1°C in the cylindrical fin channel, to merely 14°C in design B at $Re$ = 3040. Note that design B reduces $\Delta T$ by nearly 20% without an appar-

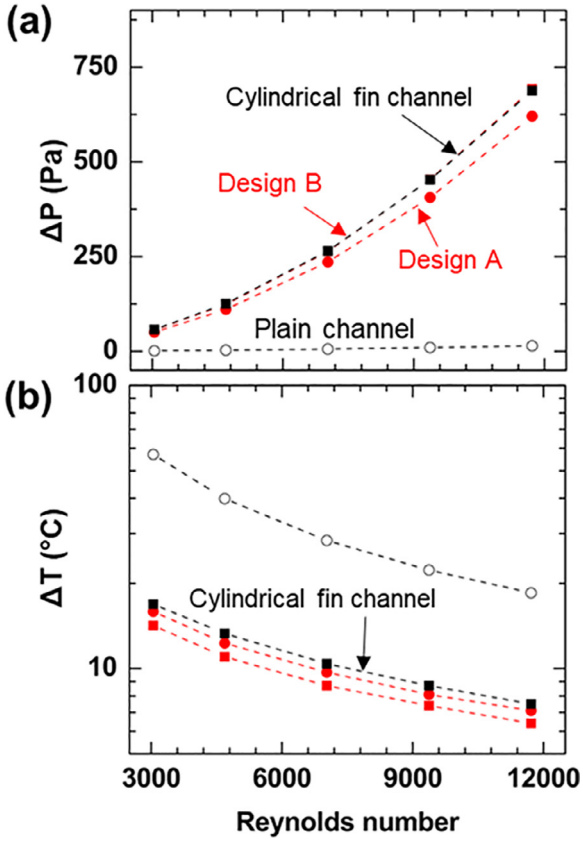


**Fig. 4.** Predicted (a) pressure drop and (b) increase of the heated surface temperature of the channels integrated with various pin fins.

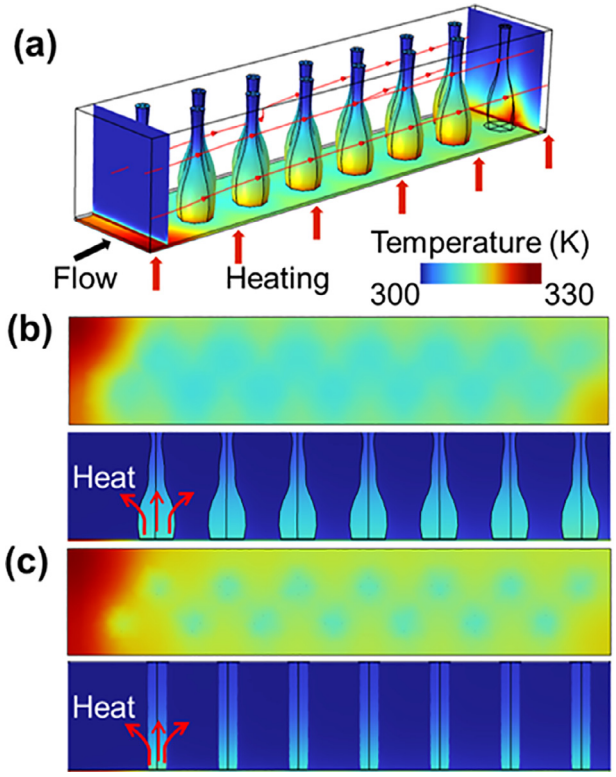


**Fig. 5.** Temperature distributions predicted for (a, b) design B, and (c) cylindrical fin channel at Re = 3040: (a) 3D diagonal view, (b, c) bottom (top) and side (bottom) views.

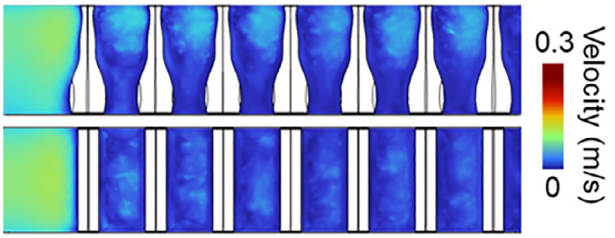


**Fig. 6.** Velocity distributions predicted for design B and cylindrical fin channel at Re = 3040 that are shown from the side of the channels.

ent increase of $\Delta P$ as compared to the cylindrical fin channel. The plain channel presents a three-fold greater $\Delta T$ than design B.

To understand how the heat transfer performance is improved in design B, we examine the temperature distributions in the heated wall and fins as shown in Fig. 5. Fig. 5(a) shows the 3D temperature distribution at $Re = 3040$. Near the channel inlet, heated coolant flow is simply concentrated within the thermal boundary layer [25], while heat does not effectively diffuse into the majority of the coolant fluid. However, with the pin fins, heat conducts through the fins and gradually diffuses into the thicker layer of fluid as shown in the temperature slice at the channel exit. In the cylindrical fin channel, a similar phenomenon occurs as shown in Fig. 1(a), although the heat diffusion layer is apparently thinner than the layer of design B. In Fig. 5(b) and 5(c), design B exhibits a more uniform temperature distribution on the heated surface and higher temperature in fins than in the cylindrical fin channel. The comparison shows that the wide bottom area of the fins apparently enhances the amount of heat transferred to the high point in the fins and to the coolant flow.

For the pin fin design, it is important to reduce the area near the unheated channel surface to minimize pressure loss. Fig. 6 shows the predicted velocity distribution within design B and the cylindrical fin channel. Since design B possesses a narrower upper area and wider lower area than the cylindrical fin channel, design B exhibits greater flow velocity in the upper channel region and smaller velocity in the lower channel region than the circular pin channel, resulting in similar mean velocity in both channels. As a result, design B presents a similar pressure drop to the cylindrical channel, which would not have been achieved by simply widening the cylindrical fins.

## 5. Machine learning model

In this section, we explore an ML model, an RF regressor, to replace the FEM-based design evaluation and expedite the optimization process. The RF regressor and GA are implemented in the open-source Scikit-learn and PyGAD Python packages [26]. Fig. 7 presents the training process of the RF regressor. First, the training dataset is prepared that tabulates the input variables and output labels. The input variables are the radial positions of 7 control points (X1 to X7) for all the pin fin designs generated in the previous section as shown in Fig. 3 and *Re* of the coolant flow. The output labels are $T$ and $\Delta P$ of the corresponding input variables, which are the FEM results acquired in the previous section as shown in Fig. 4. To reduce the time and avoid the underfitting issues in ML training, the amount and diversity of the dataset must be well determined [27]. This work employed 180 examples created from 36 pin fin geometries and 5 different *Re*. The boundary conditions are the same as the ones described in the previous section. From the dataset, the model randomly selects 80% of data for training and the remaining 20% for testing. Next, the bootstrap method is used to draw the random subsets of the training data

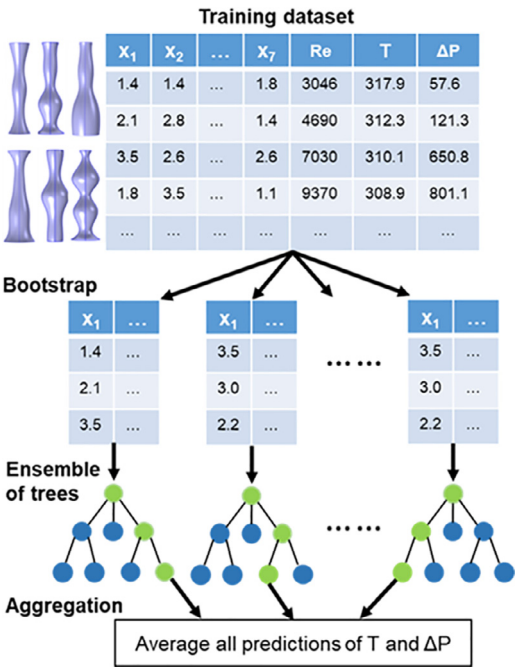


**Fig. 7.** Training process of a random forest regressor.

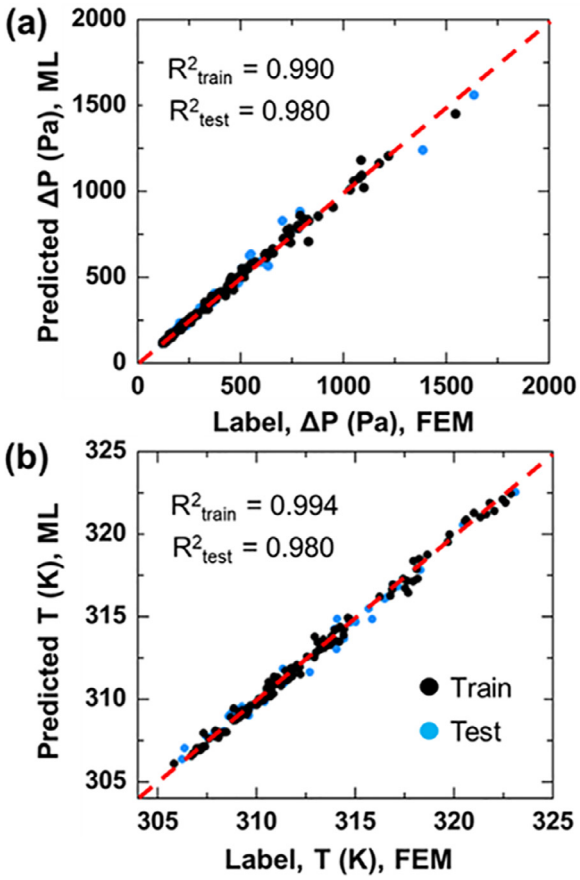


**Fig. 8.** (a) Pressure drop and (b) the heated surface temperature predicted by FEM (denoted as label) and an ML regressor.

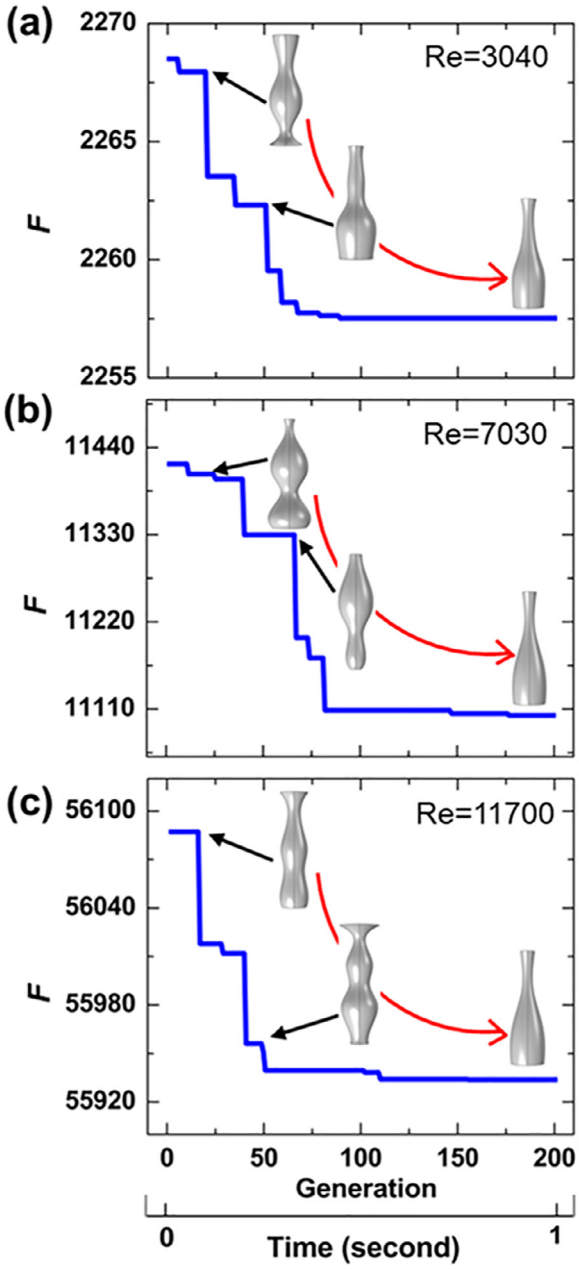


**Fig. 9.** Fitness function over generations and computation time at Re of (a) 3040, (b) 7030, and (c) 11700. For the design exploration, ML regressor served the design evaluator, while employing λ of (a) 7, (b) 35, and (c) 180 with a population size of 100.

and assign them to the decision trees. Then, the predictions of individual trees are averaged to obtain the ensemble prediction [28]. For training the decision trees, important hyperparameters are the number of trees and a seed number to initialize the random number generator. In this work, 100 trees and a seed number of 42 provided sufficient accuracy. Thus, all subsequent ML regression used these hyperparameter values. Fig. 8 compares $\Delta P$ and $T$ predicted by the trained RF regressor and FEM. The RF regressor exhibits a good accuracy for both training and testing with $R^2 > 0.99$ for the training dataset and $R^2 = 0.98$ for the testing dataset.

## 6. Optimization with GA and ML

Fig. 9 shows the best $F$ over 200 generations of evolution at three different $Re$ when the RF regressor is employed as the design

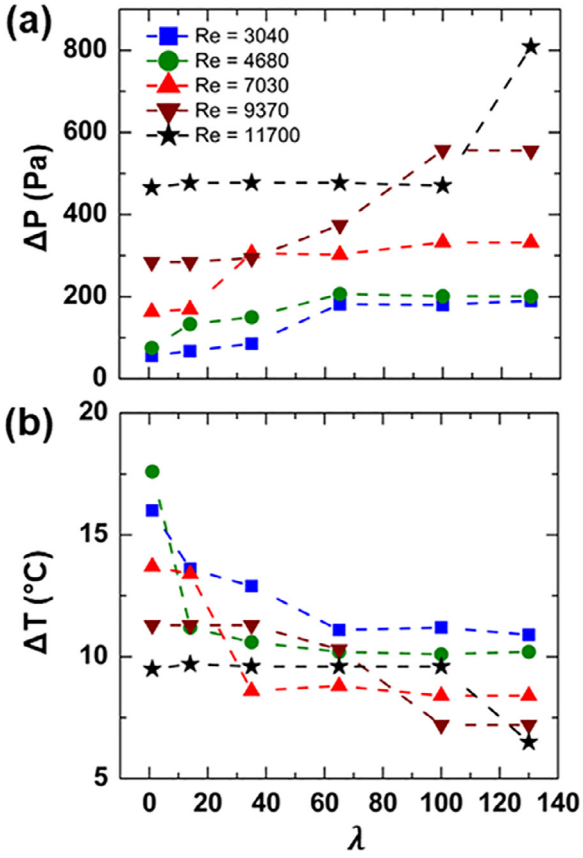


**Fig. 10.** Predicted (a) pressure drop and (b) increase of the heated surface temperature of the channels integrated with optimally designed pin fins. The ML regressor evaluated the fin performances that were designed with various λ at selected Re.

evaluator. Since the RF regressor predicts within a second, we can employ a large population of 100 for the GA, which is five times greater than that used for the optimization with FEM. Overall, the optimal designs are similar in shape and size at three different $Re$. The optimal designs were obtained after around the 100$^{th}$ generation, whereas the optimization with FEM required only around 4 generations to derive a similar design. For a relatively simple optimization problem, the GA may convert faster when using a smaller population.

The optimization at greater $Re$ requires selecting a larger λ since $\Delta P$ significantly increases with $Re$ while $T$ does not vary much. To understand how to select λ for various $Re$, we examined $\Delta P$ and $\Delta T$ of the optimal designs as a function of λ as shown in Fig. 10. In general, the optimal designs obtained with a greater λ suppresses $\Delta T$ more effectively with the cost of increased $\Delta P$ than the designs obtained with a smaller λ. For instance, at $Re = 3040$, the increase of λ from 1 to 38 reduces $\Delta T$ by 3°C with the increase of $\Delta P$ by 20 Pa. Thus, when selecting λ, it is recommended to consider both the dependence of $\Delta T$ and $\Delta P$ on λ and the design requirements.

In this work, we select λ as 7 at $Re = 3040$, 35 at $Re = 7030$, and 180 at $Re = 11790$, which provides similar designs at all three $Re$. Interestingly, due to the randomness in the RF regressor, the optimization generates slightly different designs for every execution. Thus, we repeated the optimization 10 times for each $Re$, selected similar designs out of the 10 designs, and took their average shape as a final solution. In particular, we denote the solution for $Re = 3040$ as design C for the comparison in the following section. From the repetitive optimization tasks, we observed that the design evaluation by RF regression was instantaneous, allowing us

to complete the 30 optimizations in less than one minute in our computer setting which could take over a month with the GA combined with FEM.

## 7. Comparison of optimized pin fins against other designs

To understand how the optimization enhances the performance of pin fins, we calculate the convection heat transfer coefficient ($h$) and friction factor ($f$) of the optimal designs as shown in Fig. 11 as a function of $Re$. Fig. 11(a) shows $h$ computed by $h = q''/(T\text{-}T_m)$, where $T_m$ is the mean temperature of the working fluid. First, to verify our FEM, we compare $h$ of the plain channel with the Sieder-Tate correlation [29]. The two optimal designs obtained with $\lambda = 7$ (i.e., design B and design C) exhibit very similar $h$ with a percent error of less than 2% because their shapes are close to each other. Design B and C are superior to other designs since their $h$ is 4 times greater than $h$ of the plain channel and 20 - 30% greater than $h$ of the cylindrical fin channel in the corresponding range of $Re$ (i.e., $Re$ = 3040 - 11790). Similarly, $h$ of design A is 10% higher than that of the cylindrical pin fin.

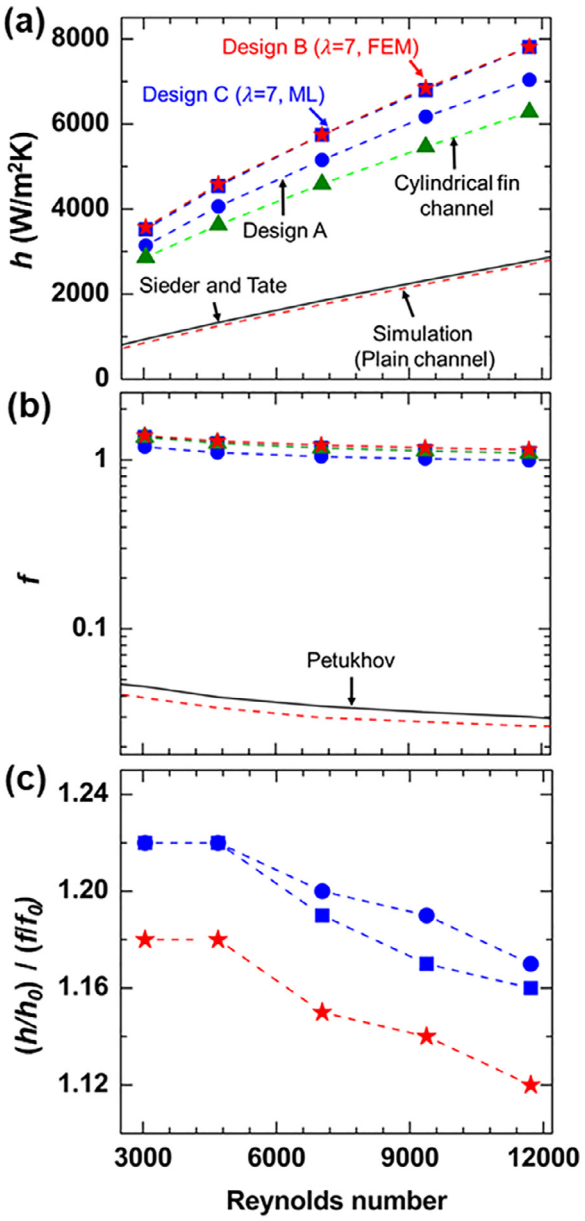


**Fig. 11.** Comparison of (a) convection heat transfer coefficients, (b) friction factors, and (c) efficiency index of the channels integrated with optimal pin fins along with the circular pin fin channel.

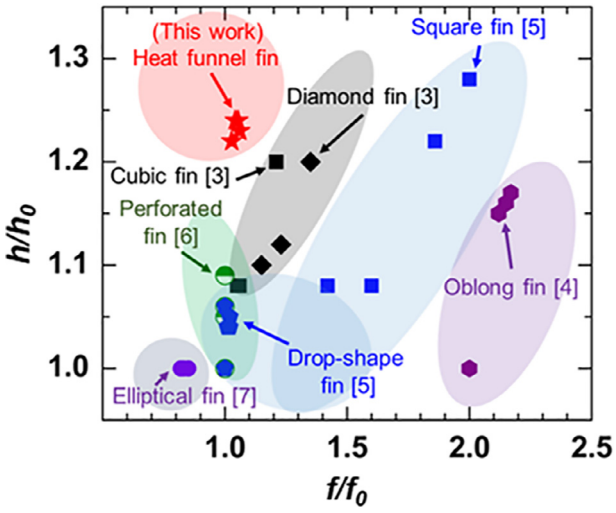


**Fig. 12.** Comparison of the current work and previous studies with different pin fin designs. The fin shapes with large heat transfer coefficients and small friction factors are desirable which tend to locate on the top and left sides of the plot.

Fig. 11(b) compares $f$ of channels as a function of $Re$. For the estimation of $f$, we use Darcy-Weisbach equation $f = 2\Delta P D_h/(\rho u^2 L)$, where $D_h$ is the hydraulic diameter of the channel. The comparison of $f$ between the FEM simulation of the plain channel and Petukhov correlation validates the FEM accuracy. Despite the similar designs, $f$ of design C is 4% more than $f$ of design B. An interesting fact is that design B, design C, and the standard cylindrical fin channel all exhibit similar $f$ although design B and design C show superior $h$ to the $h$ of the cylindrical fin channel ($h_0$). Design A presents the smallest $f$ among the pin fin designs which is around 12% smaller than $f$ of the cylindrical fin channel ($f_0$). Another important metric for the heat transfer enhancement techniques is the efficiency index [30] which is defined as $\eta = (h/h_0)/(f/f_0)$, representing the heat transfer enhancement ratio per friction factor increase ratio. As shown in Fig. 11(c), design A exhibits the largest efficiency index, $\eta$ = 1.18-1.22, in the range of $Re$ from 3034 to 11790. Designs B and C also achieve $\eta > 1$ by giving $\eta$ = 1.16 - 1.22 for designs B and $\eta$ = 1.12 - 1.18 for design C.

Fig. 12 shows a comparison between the optimally designed pin fins (denoted as heat funnel fin) against other fins with standard shapes, focusing on $h/h_0$ and $f/f_0$ [3–7]. While the rounded fins such as elliptical, drop-shaped, cylindrical perforated fins exhibit small $f/f_0$, their $h/h_0$ is 7% - 20% lower than that of heat funnel fins. The noncircular-shaped fins such as cubic, diamond, and square fins may offer similar $h/h_0$ as compared to the heat funnel fins, but their $f/f_0$ is approximately 30 - 80% greater.

For the application of the pin fins with a nonstandard shape, it is important to examine if there are any concentrated thermal stresses. Stress tends to concentrate in regions with irregular geometries. Fig. 13(a) shows the stress distribution in design B predicted by a FEM that is implemented in Abaqus 2021. Two ends of the fin are mechanically fixed, while the bottom end is subject to a constant of heat flux, $q''$ = 5 W/cm$^2$. On the lateral area of the fin, the convection heat transfer coefficient is assumed as 400 W/m$^2$K to create a similar temperature distribution of the fins shown in Fig. 5(a) with the highest temperature of 325K. The simulation shows that the maximum stress occurs at the fin bottom region which is mechanically fixed with the highest temperature. The predicted maximum stress is 18 MPa for design A, 35 MPa for design B, and 10 MPa for the cylindrical pin fin. Such thermal

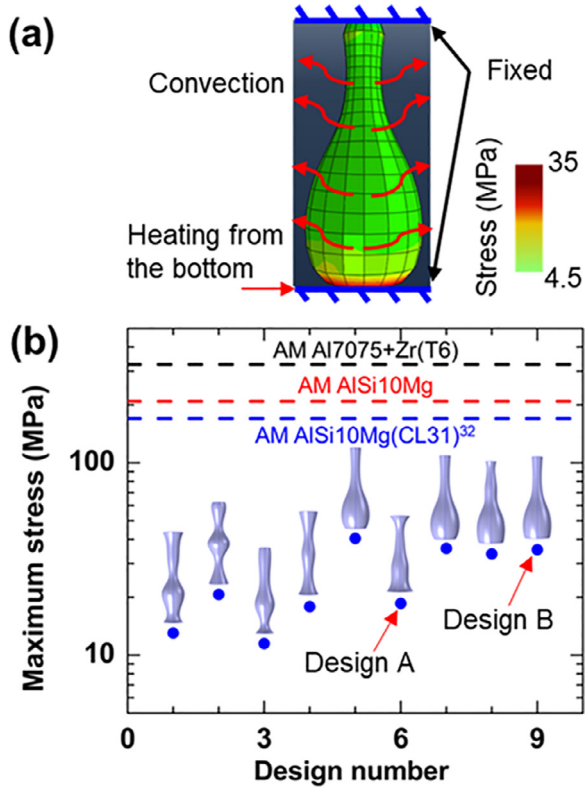


**Fig. 13.** (a) Stress distribution in design B. (b) Comparison of the maximum thermal stresses predicted for various fin designs with the yield strengths of 3D printed aluminum alloys.

stress levels are lower than the yield strengths of 3D printed aluminum alloys [31] as shown in Fig. 13(b). The yield strength of the selected aluminum alloys ranges from 170 to 370 MPa, indicating that the heat funnel fins that are made of 3D printed aluminum alloys will be mechanically robust under the thermofluidic conditions considered in this work.

## 8. Conclusion

We optimized the shapes of a pin fin array integrated in a channel for the *Re* between 3000 and 12000. For the optimization, the GA is coupled to either a CFD simulation model or an ML regressor to automatically search the shapes of the pin fins. The ML regressor evaluated the temperature and pressure of the finned channel within a second, and enabled us to employ a large population in the GA, and identified a GA parameter $\lambda$ for various *Re*. The optimization identified a funnel shape of pin fins (heat funnel fin) that improved the heat transfer coefficient by approximately 20% without an apparent increase of pressure drop penalty as compared to the standard cylindrical pin fin. Compared to the other conventional non-circular pin fins, the heat funnel fin exhibits an 18% greater heat transfer coefficient when the friction factor increase is limited below 20%. The approach that combines GA and an ML regressor can be extended to optimize the designs of a variety of heat transfer systems where the CFD simulation may take a tremendous amount of time for computation. The experimental validation of the heat funnel fin is also an interesting extension of this work by prototyping the fins using additive manufacturing.

## CRediT authorship contribution statement

**Nam Phuong Nguyen:** Modeling, Designing and Writing. **Elham Maghsoudi:** Supervision and Reviewing. **Scott N. Roberts:** Supervision and Reviewing. **Beomjin Kwon:** Supervision, Writing, Reviewing and Editing.

## Declaration of Competing Interest

The authors declare the following financial interests/personal relationships which may be considered as potential competing interests:

Nam Phuong Nguyen reports financial support was provided by Jet Propulsion Laboratory.

## Data availability

Data will be made available on request.

## Acknowledgments

This research was supported by a grant from Strategic University Research Partnership (RSA 1670129) from the Jet Propulsion Laboratory, California Institute of Technology, under contract with the National Aeronautics and Space Administration (80NM0018D0004).

## References

[1] M. Ebadian, C. Lin, A review of high-heat-flux heat removal technologies, J. Heat Transfer 133 (11) (2011).
[2] A. Hehr, et al., Hot isostatic pressing of ultrasonic additive manufacturing liquid cold plate heat exchangers, J. Spacecr. Rocket. 58 (3) (2021) 910–914.
[3] M. Chyu, C. Yen, S. Siw, Comparison of heat transfer from staggered pin fin arrays with circular, cubic and diamond shaped elements, Turbo Expo: Power for Land, Sea, and Air, 2007.
[4] Metzger, D., C. Fan, and S. Haley, *Effects of pin shape and array orientation on heat transfer and pressure loss in pin fin arrays.* 1984.
[5] N. Sahiti, et al., Performance comparison of pin fin in-duct flow arrays with various pin cross-sections, Appl. Therm. Eng. 26 (11-12) (2006) 1176–1192.
[6] A.B. Dhumne, H.S. Farkade, Heat transfer analysis of cylindrical perforated fins in staggered arrangement, Int. J. Innov. Technol. Explor. Eng. 2 (5) (2013) 225–230.
[7] L. Huang, Q. Li, H. Zhai, Experimental study of heat transfer performance of a tube with different shaped pin fins, Appl. Therm. Eng. 129 (2018) 1325–1332.
[8] Y. Cormier, et al., Additive manufacturing of pyramidal pin fins: Height and fin density effects under forced convection, Int. J. Heat Mass Transfer 75 (2014) 235–244.
[9] S. Mohsin, A. Maqbool, W.A. Khan, Optimization of cylindrical pin-fin heat sinks using genetic algorithms, IEEE Trans. Compon. Packag. Technol. 32 (1) (2009) 44–52.
[10] T. Wu, B. Ozpineci, C. Ayers, Genetic algorithm design of a 3D printed heat sink, 2016 IEEE Applied Power Electronics Conference and Exposition (APEC), IEEE, 2016.
[11] G. Xie, B. Sundén, Q. Wang, Optimization of compact heat exchangers by a genetic algorithm, Appl. Therm. Eng. 28 (8-9) (2008) 895–906.
[12] H. Moon, et al., Ultra-power-dense heat exchanger development through genetic algorithm design and additive manufacturing, Joule 5 (11) (2021) 3045–3056.
[13] F. Almeida, A. Awruch, Design optimization of composite laminated structures using genetic algorithms and finite element analysis, Compos. Struct. 88 (3) (2009) 443–454.
[14] T. Ma, et al., Recent trends on nanofluid heat transfer machine learning research applied to renewable energy, Renew. Sustain. Energy Rev. 138 (2021) 110494.
[15] Z.Q. Fard, Z.S. Zomorodian, S.S. Korsavi, Application of machine learning in thermal comfort studies: A review of methods, performance and challenges, Energy Build. (2021) 111771.
[16] M.H. Ahmadi, et al., Applications of machine learning methods in modeling various types of heat pipes: a review, J. Therm. Anal. Calorim. 146 (6) (2021) 2333–2341.
[17] M. Kang, L.K. Hwang, B. Kwon, Machine learning flow regime classification in three-dimensional printed tubes, Phys. Rev. Fluids 5 (8) (2020) 081901.
[18] Y. Suh, R. Bostanabad, Y. Won, Deep learning predicts boiling heat transfer, Sci. Rep. 11 (1) (2021) 5622.
[19] B. Kwon, F. Ejaz, L.K. Hwang, Machine learning for heat transfer correlations, Int. Commun. Heat Mass Transfer 116 (2020) 104694.
[20] T.-M. Jeng, S.-C. Tzeng, Pressure drop and heat transfer of square pin-fin arrays in in-line and staggered arrangements, Int. J. Heat Mass Transfer 50 (11-12) (2007) 2364–2375.
[21] F.E. Ames, L.A. Dvorak, M.J. Morrow, Turbulent Augmentation of Internal Convection Over Pins in Staggered-Pin Fin Arrays, J. Turbomach. 127 (1) (2005) 183–190.

[22] Kumar, M., et al., *Genetic algorithm: Review and application*. Available at SSRN 3529843, 2010.
[23] T. Menrath, et al., Shape Optimization of a Pin Fin Heat Sink, 2020 36th Semiconductor Thermal Measurement, Modeling & Management Symposium (SEMI-THERM), IEEE, 2020.
[24] F. Hajabdollahi, et al., Multi-objective optimization of pin fin to determine the optimal fin geometry using genetic algorithm, Appl. Math. Modell. 36 (1) (2012) 244–254.
[25] B. Kwon, et al., Heat transfer enhancement of internal laminar flows using additively manufactured static mixers, Int. J. Heat Mass Transfer 137 (2019) 292–300.
[26] F. Pedregosa, et al., Scikit-learn: machine learning in Python, J. Mach. Learn. Res. 12 (2011) 2825–2830.
[27] X. Ying, An overview of overfitting and its solutions, Journal of physics: Conference series, IOP Publishing, 2019.
[28] X. Dong, et al., A survey on ensemble learning, Front. Comput. Sci. 14 (2) (2020) 241–258.
[29] E.N. Sieder, G.E. Tate, Heat transfer and pressure drop of liquids in tubes, Indus. Eng. Chem. 28 (12) (1936) 1429–1435.
[30] K.L. Kirsch, K.A. Thole, Pressure loss and heat transfer performance for additively and conventionally manufactured pin fin arrays, Int. J. Heat Mass Transfer 108 (2017) 2502–2513.
[31] J.H. Martin, et al., 3D printing of high-strength aluminium alloys, Nature 549 (7672) (2017) 365–369.